

# RSC Advances



This is an *Accepted Manuscript*, which has been through the Royal Society of Chemistry peer review process and has been accepted for publication.

*Accepted Manuscripts* are published online shortly after acceptance, before technical editing, formatting and proof reading. Using this free service, authors can make their results available to the community, in citable form, before we publish the edited article. This *Accepted Manuscript* will be replaced by the edited, formatted and paginated article as soon as this is available.

You can find more information about *Accepted Manuscripts* in the [Information for Authors](#).

Please note that technical editing may introduce minor changes to the text and/or graphics, which may alter content. The journal's standard [Terms & Conditions](#) and the [Ethical guidelines](#) still apply. In no event shall the Royal Society of Chemistry be held responsible for any errors or omissions in this *Accepted Manuscript* or any consequences arising from the use of any information it contains.

## ARTICLE

# Formation, structure and electrochemical performance of the nano-sized $\text{Li}_2\text{FeSiO}_4/\text{C}$ synthesized with the co - incorporation of citric acid and glucose followed by a two – step annealing

Cite this: DOI: 10.1039/x0xx00000x

Received 00th September 2014,  
Accepted 00th September 2014

DOI: 10.1039/x0xx00000x

www.rsc.org/

L. Mi<sup>a</sup>, H. Q. Liu<sup>a</sup>, R. Y. Tian<sup>a</sup>, Y. Jiang<sup>a</sup>, L. N. Zhang<sup>b,c</sup>, X. H. Gu<sup>c</sup>, Y. J. Guo<sup>a</sup>, H. F. Wang<sup>a\*</sup>, L. F. Sun<sup>a\*</sup> and W. G. Chu<sup>a\*</sup>

Nano-sized  $\text{Li}_2\text{FeSiO}_4/\text{C}$  composites are synthesized using a simple recipe via the co - incorporation of citric acid and glucose with various molar ratios followed by a two-step annealing. Citric acid and glucose traditionally recognized as reducing agents, size reduction agents and carbon sources are found to play different roles here in which glucose has a far more effective and critical role to play in size reduction and citric acid alleviates the agglomeration of nanoparticles more effectively, different than before. It is reported for the first time that the decrease in intensity ratio between the reflections around  $2\theta = 24.3^\circ$  and  $33.1^\circ$  of monoclinic  $\text{Li}_2\text{FeSiO}_4$  with space group of  $P2_1$  with the increased amount of citric acid and glucose originates from the increased intermixing occupancies between Fe and Li. An appropriate intermixing occupancy between Fe and Li could facilitate the electrochemical performance of  $\text{Li}_2\text{FeSiO}_4$ . This study provides a new idea to optimize the electrochemical performance of  $\text{Li}_2\text{FeSiO}_4$  by controlling the intermixing occupancy of Fe and Li through introducing some organic substances during synthesis.

## 1. Introduction

Lithium-ion batteries (LIBs) have been attracting great interest due to their good performance, long life time and environmental friendliness.<sup>1-3</sup> As the most important component of LIBs cathode materials are extensively explored such as layered  $\text{LiCoO}_2$ , spinel  $\text{LiMn}_2\text{O}_4$ , olivine  $\text{LiFePO}_4$ , monoclinic  $\text{LiFeBO}_3$ , polymorphic  $\text{Li}_2\text{FeSiO}_4$  and their derivatives<sup>4-8</sup> However,  $\text{Li}_2\text{FeSiO}_4$  is unique due to a high theoretical specific capacity as a result of possible two  $\text{Li}^+$  extraction (166 and 332  $\text{mAhg}^{-1}$  for one and two  $\text{Li}^+$  extraction, respectively)<sup>9,10</sup> and a stable structure attributable to the strong Si - O bonds albeit having different crystal structures determined by different treatments.<sup>11-14</sup>

Even so,  $\text{Li}_2\text{FeSiO}_4$  is shown to have poor electronic conductivity and sluggish ion diffusion, and thus exhibits poor electrochemical performance, particularly at relatively low temperatures and even at room temperature.<sup>15, 16</sup> Normally, the performance of  $\text{Li}_2\text{FeSiO}_4$  can be improved by both enhancing the  $\text{Li}^+$  transport through reducing the size of particles<sup>17 - 19</sup> and increasing the electronic conductivity through encapsulating particles with conductive films, such as carbon.<sup>20-23</sup> However, Little is known about structural defects and their influences on the electrochemical performance, especially so called  $\text{Fe}_{\text{Li}}$  ( $\text{Li}_{\text{Fe}}$ ) antisite defects (partial occupation of Fe (Li) at the Li (Fe) site). Indeed, the occupation of M (Fe, Co and Mn) at the Li site is generally thought to have a negative effect on the electrochemical performance due to the blocking effect of  $\text{Li}^+$  transport caused by the presence of M, as already reported in layered  $\text{LiCoO}_2$ , spinel  $\text{LiMn}_2\text{O}_4$  and olivine

$\text{LiFePO}_4$ .<sup>24-26</sup> In sharp contrast, the role of the occupation of Li at the M (M = Fe, Co or Mn) site on the electrochemical performance is scarcely touched. For  $\text{Li}_2\text{FeSiO}_4$  the correlations between the capacity and the structure properties, rather the Fe - Li antisite defects involved are not elucidated as yet though relatively high capacities with more than one  $\text{Li}^+$  extraction were achieved<sup>27-30</sup> The structural rearrangement during the first charging process gives a hint that whether or not more than one  $\text{Li}^+$  extraction may be related to the Fe - Li antisite defects present in  $\text{Li}_2\text{FeSiO}_4$ .<sup>31</sup> At present, for  $\text{Li}_2\text{FeSiO}_4$  both the capacity and the rate performance are still far from satisfactory.<sup>32</sup> In depth understanding of its structural properties and their influences on the electrochemical performance would undoubtedly be greatly helpful for enhancing the performance.

Herein we developed a simple way to synthesize  $\text{Li}_2\text{FeSiO}_4/\text{C}$  nanoparticles with different sizes and different intermixing occupancies between Fe and Li by introducing citric acid and glucose in different molar ratios. Citric acid serves to suppress the growth of  $\text{Li}_2\text{FeSiO}_4$  particles and form a porous structure.<sup>33-35</sup> Both citric acid and glucose can be taken as the source of conductive carbon. The combination of citric acid and glucose has a profound effect on not only the growth kinetics but also the formation of structural defects of  $\text{Li}_2\text{FeSiO}_4$  particles. We reported the variation of the intermixing occupancies between Fe and Li with the molar ratios of citric acid to glucose, the roles of citric acid and glucose, and their dependence of the electrochemical performance.

## 2. Experimental

## 2.1 Materials synthesis

Nanosized  $\text{Li}_2\text{FeSiO}_4/\text{C}$  composites were prepared using a sol-gel method with analytically graded  $\text{LiNO}_3$ ,  $\text{Fe}(\text{NO}_3)_3 \cdot 9\text{H}_2\text{O}$  and Nano- $\text{SiO}_2$  as reactants according to the stoichiometric ratio of 2:1:1. Firstly, 0.02 mol nano- $\text{SiO}_2$  was added into 30ml deionized water followed by ultrasonication for 2h to form a uniform emulsion. Then, 0.04 mol  $\text{LiNO}_3$ , 0.02 mol  $\text{Fe}(\text{NO}_3)_3 \cdot 9\text{H}_2\text{O}$ , citric acid and glucose with various molar ratios were added into the above emulsion in sequence, and the mixture thus obtained was magnetically stirred for 12 h to form a solution. During the preparations, the molar ratio of resulted  $\text{Li}_2\text{FeSiO}_4$ , citric acid and glucose is 15 :  $x$  :  $y$  in which  $x$  and  $y$  are varied (when  $x = 3, y = 8, 9, 10$  and  $11$ , respectively, labeled by C3G8, C3G9, C3G10 and C3G11; when  $x = 6, y = 5, 6, 7, 8, 9$  and  $10$ , respectively, labeled by C6G5, C6G6, C6G7, C6G8, C6G9 and C6G10; when  $x = 9, y = 5, 6$  and  $7$ , respectively, labeled by C9G5, C9G6 and C9G7; C: citric acid and G: glucose). Finally, the solution was water bathed at  $80^\circ\text{C}$  until it was dried. The dried precursor was grinded and subsequently heated at  $200^\circ\text{C}$  for 6 h in a tube furnace under the flowing argon, followed by further treatment at  $600^\circ\text{C}$  for 4 h. After the furnace was cooled down to room temperature  $\text{Li}_2\text{FeSiO}_4/\text{C}$  composites were collected.

## 2.2 Materials characterizations

The structure of  $\text{Li}_2\text{FeSiO}_4/\text{C}$  samples was characterized by X-ray diffraction technique (XRD). The XRD data were collected on a diffractometer (D/MAX-TTRIII (CBO), Rigaku Corporation, Japan) with a Cu  $K\alpha$  radiation at 50 kV and 300 mA. The data for Rietveld refinements were recorded from  $15^\circ$  to  $120^\circ$  with a step size of  $0.02^\circ$ , and a step time of 4s. The morphology and structure of samples was studied by Field emission scanning electron microscopy (FESEM, Sirion 200, FEI Company, USA), transmission electron microscopy (TEM) and high resolution transmission electron microscopy (HRTEM, Tecnai F20, FEI Company, USA). The carbon content in the resulted  $\text{Li}_2\text{FeSiO}_4/\text{C}$  composites was determined using a carbon and sulfur analyzer (CS-344, LECO Company, USA).

Mössbauer measurement was made using a 512 - channel Mössbauer spectrometer (MS - 500, Oxford Instrument Company, United Kingdom) working in a constant acceleration mode with a  $^{57}\text{CoRh}$  source and a transmission geometry at room temperature with a calibration spectrum for  $\alpha$  - Fe foil.

## 2.3 Electrochemical measurements

The electrochemical study was carried out using CR 2025 coin cell. The  $\text{Li}_2\text{FeSiO}_4/\text{C}$  composite, acetylene black and PVDF (poly(vinylidene fluoride)) were mixed with a weight ratio of 75 : 15 : 10, and then grinded using NMP (N-methyl-2-pyrrolidone) as the solvent. The resulted slurry was pasted onto an aluminum foil and dried under vacuum at  $110^\circ\text{C}$  for 12 h. Then the foil was punched into circular cathode and pressed under 20 MPa. The cells were assembled in an argon - filled glove box with a lithium metal as counter electrode and Celgard 2316 as a separator. The electrolyte was 1mol/L  $\text{LiPF}_6$  dissolved in a mixture of EC (ethylene carbonate), EMC (ethyl methyl carbonate) and DMC (dimethyl carbonate) with a volume ratio of 1 : 1 : 1. Electrochemical measurements were performed on a battery test system (BTS - 5 V, Neware Company, China) at room temperature ( $25^\circ\text{C}$ ). Both cyclic voltammetric (CV) data and electrochemical impedance spectra (EIS) were collected using an electrochemical workstation (CHI660D, Shanghai Chenchua Company, China).

## 3 Results and discussion

### 3.1 Structure analysis

To identify the structure of the synthesized products, their XRD data are shown in Figure 1a. All the XRD patterns are found to be in accordance with those reported in ref. 9, indicating that  $\text{Li}_2\text{FeSiO}_4$  is the primary phase with minor impurities such as  $\text{Li}_2\text{SiO}_3$  and  $\text{LiFe}_3\text{O}_4$  involved in some samples. However, small humps around  $25^\circ$  suggest the possible presence of amorphous phase in these samples. Careful inspection reveals that samples C3G8, C6G8, C6G9 and C6G10 are of much better purity. All the samples show very close peak positions, implying similar lattice parameters. However, an unusual point is that the relative intensity of the reflections around  $2\theta = 24.3^\circ$  and  $33.1^\circ$  differs for different samples, as outlined in Table 1. The intensity ratio tends to drop as the total molar quantity of citric acid and glucose increases. In addition, the breadths of the reflections change with the samples. The crystallite size can be estimated according to the Scherrer's formula  $D = k\lambda/B\cos\theta$  in which  $k$  is the Scherrer constant, 0.89,  $\lambda$  the X-ray wavelength, 1.54056 Å,  $B$  the full width at half height of a reflection and  $\theta$  the diffraction angle.<sup>36</sup> We derive the average sizes of crystallites along the directions normal to the reflections of  $2\theta = 16.5^\circ$  and  $24.3^\circ$ , ranging from about 17 to 35 nm, as given in Table 1. Their sizes along the two directions are very similar, suggesting sphere - like nanoparticles. The size of crystallites decreases as the total molar quantity of citric acid and glucose increases, which is readily understandable. However, with their total molar quantity fixed the average size is found to increase with the amount of citric acid, which is quite unusual and different from the traditional viewpoints.<sup>33</sup> Therefore, glucose is really responsible for size reduction in the presence of citric acid, which is indeed beyond our initial expectation. This may be related to more hydroxyl groups terminated for glucose and the interaction between glucose and citric acid during the synthesis. The exact underlying mechanism remains to be resolved.

To better understand the structure of the  $\text{Li}_2\text{FeSiO}_4/\text{C}$ , higher quality XRD data of samples C3G8, C6G9 and C6G10 are presented in Figure 1b. A monoclinic structural model with space group  $P2_1$  reported in ref. 37 was employed to perform Rietveld refinements on the XRD data.<sup>38</sup> The simulated and experimental patterns agree well, as clearly revealed by the XRD data between  $80^\circ$  and  $120^\circ$  in the enlarged insets. Some of the refined parameters are outlined in Table 2 and the atomic coordinates are shown in Table 1S in supporting information. In fact, other monoclinic structural models with space groups  $P2_1/n$  and  $Pmn2_1$  reported in refs. 13 and 39 were also tried as a single phase or as one of coexistent phases, but their refinement results are not as good as those based on space group  $P2_1$ . The weight percentage of the impurities is estimated to be 0.69 %, 1.40 % and 0.75 % for samples C3G8, C6G9 and C6G10, respectively. The lattice parameters for three samples are a little bit different, but quite close to those reported in ref 37. The large X-ray scattering contrast between Fe and Li allows one to refine the intermixing occupancies at the Li and Fe sites with full occupations. According to the refined occupancies shown in Table 1S (The results for sample C9G7 are also given to show the changing tendency of the intermixing occupancies.) the chemical formulae were derived to be  $(\text{Li}_{1.916}\text{Fe}_{0.084})(\text{Fe}_{0.806}\text{Li}_{0.194})\text{SiO}_4$  ( $\text{Li}_{2.110}\text{Fe}_{0.890}\text{SiO}_4$ ),  $(\text{Li}_{1.864}\text{Fe}_{0.136})(\text{Fe}_{0.591}\text{Li}_{0.409})\text{SiO}_4$  ( $\text{Li}_{2.273}\text{Fe}_{0.727}\text{SiO}_4$ ),  $(\text{Li}_{1.827}\text{Fe}_{0.173})(\text{Fe}_{0.549}\text{Li}_{0.451})\text{SiO}_4$  ( $\text{Li}_{2.278}\text{Fe}_{0.722}\text{SiO}_4$ ) and  $(\text{Li}_{1.773}\text{Fe}_{0.227})(\text{Fe}_{0.466}\text{Li}_{0.534})\text{SiO}_4$  ( $\text{Li}_{2.307}\text{Fe}_{0.693}\text{SiO}_4$ ) for samples C3G8, C6G9, C6G10 and C9G7, respectively. Obviously, the intermixing occupation between Fe and Li is enhanced with the molar quantity of citric acid and glucose. From Table 1S one can conclude that Fe and Li tend to preferentially replace Li and Fe in the order of Li3, Li4, Li2 and Li1 as well as Fe1 and Fe2 sites, respectively. Consequently, the increased intermixing occupancies

## RSC advances

ARTICLE

are responsible for the decreased intensity ratio of the reflections around  $2\theta = 24.3^\circ$  and  $33.1^\circ$  aforementioned.

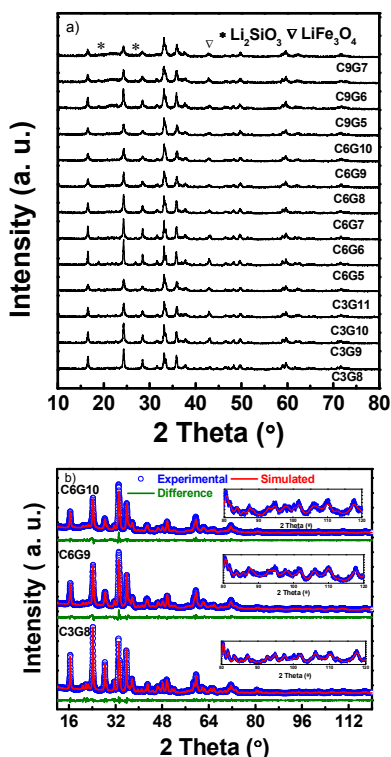


Figure 1. (a) The experimental XRD patterns of samples C3G8, C3G9, C3G10, C6G5, C6G6, C6G7, C6G8, C6G9, C6G10, C9G5, C9G6 and C9G7. (b) The experimental, simulated, and different XRD patterns of samples C3G8, C6G9 and C6G10

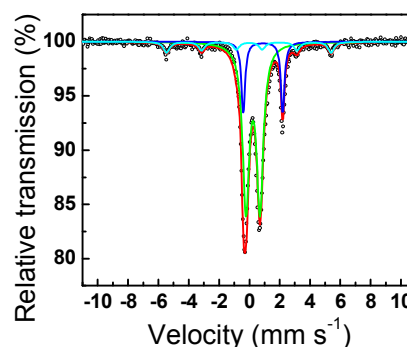
Table 1. Size of crystallites along the directions normal to (101) and (111), and the ratios of intensity of the reflections at  $2\theta = 24.3^\circ$  and  $33.1^\circ$  for all the samples

Samples	$I_{2\theta=24.3^\circ} / I_{2\theta=33.1^\circ}$	Size of crystallites along the direction normal to planes (nm)	
		(101)	(111)
C3G8	1.272	28.4	28.8
C3G9	1.184	26.9	29.1
C3G10	0.903	23.8	24.6
C3G11	0.618	18.4	19.5
C6G5	1.183	37.8	35.0
C6G6	1.102	30.5	31.5
C6G7	1.092	24.7	25.1
C6G8	0.893	18.8	20.0
C6G9	0.795	20.7	18.3
C6G10	0.628	18.3	17.2
C9G5	0.700	25.9	24.5
C9G6	0.652	22.1	19.3
C9G7	0.333	20.7	18.1

Table 2. Some parameters derived from the Rietveld refinements for samples C3G8, C6G9, C6G10 and C9G7

Samples	C3G8	C6G9	C6G10	C9G7
Parameters				
$a$ (Å)	8.2393	8.2273	8.2335	8.2171
$b$ (Å)	5.0103	4.9959	4.9961	4.9919
$c$ (Å)	8.2318	8.2387	8.2422	8.2305
$\beta$ (°)	99.1341	98.8953	98.9160	98.7333
Reliability factors				
$R_{wp}$	7.12%	6.52%	6.77%	5.50%
$R_p$	3.61%	3.47%	3.63%	2.54%
Refined formula	$(\text{Li}_{1.916}\text{Fe}_{0.084})(\text{Fe}_{0.806}\text{Li}_{0.194})\text{SiO}_4$	$(\text{Li}_{1.864}\text{Fe}_{0.136})(\text{Fe}_{0.591}\text{Li}_{0.409})\text{SiO}_4$	$(\text{Li}_{1.827}\text{Fe}_{0.173})(\text{Fe}_{0.549}\text{Li}_{0.451})\text{SiO}_4$	$(\text{Li}_{1.773}\text{Fe}_{0.227})(\text{Fe}_{0.466}\text{Li}_{0.534})\text{SiO}_4$
Refined impurity	0.69%	1.40%	0.75%	1.76%

To further understand the intermixing occupation between Fe and Li, Mössbauer spectrum for sample C6G9 was recorded at room temperature, which is shown in Figure 2. The spectrum can be fitted with  $\text{Fe}^{2+}$  and  $\text{Fe}^{3+}$  two doublets, and one  $\text{Fe}^{3+}$  sextet, and their parameters are outlined in Table 3. The sextet and the two doublets could be ascribed to an amorphous Fe rich magnetic phase and  $\text{Li}_{2.273}\text{Fe}_{0.727}\text{SiO}_4$ , respectively. The isomer shift  $\delta$ , the electric quadrupole splitting  $Q_s$  are 0.26, 0.93  $\text{mm s}^{-1}$  and 0.92, 2.6  $\text{mm s}^{-1}$ , which correspond to the  $\text{Fe}^{2+}$  and  $\text{Fe}^{3+}$  doublets, respectively, in accord with refs. 40 and 41. Analysis of the Mössbauer spectrum doesn't evidence the presence of multiple crystalline phases with different structures of  $\text{Li}_2\text{FeSiO}_4$  either, supporting the refinement results above. The quadrupole splitting is usually considered to be correlated to the degree of distortion of  $\text{FeO}_4$ .<sup>42</sup> Thus, different quadrupole splittings suggest different degrees of distortion of  $\text{FeO}_4$ . From the area ratio of  $\text{Fe}^{2+}$  and  $\text{Fe}^{3+}$  doublets the percentage of  $\text{Fe}^{3+}$  is estimated to be about 25%. However, according to the refined  $\text{Li}_{2.273}\text{Fe}_{0.727}\text{SiO}_4$  the percentage of  $\text{Fe}^{2+}$  is figured out to be about 37%. Despite some discrepancies in the quantity of  $\text{Fe}^{3+}$  a significant amount of  $\text{Fe}^{3+}$  could be concluded to remain in the lattice. This discrepancy may arise partly from not very accurate determination of Li occupancies at the different sites due to its small X-ray scattering factor. In contrast, the stoichiometry of Fe is accurate due to its much larger X-ray scattering factor. With 14.5%  $\text{Fe}^{3+}$  amorphous phase considered, the resultant chemical composition should reasonably be close to  $\text{Li}_{2.022}\text{Fe}_{1.006}\text{SiO}_4$  determined by the ICP analysis. Here, we just take sample C6G9 as an example to elucidate the intermixing occupancy between Fe and Li. The increase of the intermixing occupancy with the molar quantity of citric acid and glucose needs intensively exploring.



## ARTICLE

Figure 2. Room temperature Mössbauer spectrum for sample C6G9, the spectrum is fitted with two doublets and one sextet, which correspond to lithium iron orthosilicate with  $\text{Fe}^{2+}$  and  $\text{Fe}^{3+}$  mixed valence states and magnetic phase, respectively

Table 3. Mössbauer parameters of sample C6G9,  $H_{\text{hf}}$  is the magnetic hyperfine field,  $Q_s$  is the electric quadrupole splitting,  $\delta$  is the isomer shift,  $\Gamma$  is the peak width

	$\delta$ (mm s <sup>-1</sup> )	$Q_s$ (mm s <sup>-1</sup> )	$H_{\text{hf}}$ (kOe)	$\Gamma$ (mm s <sup>-1</sup> )	Area Ratio (%)
1 (doublet)	0.26 ± 0.00	0.93 ± 0.01	0.26 ± 0.00	0.26 ± 0.00	64.1
2 (doublet)	0.92 ± 0.00	2.60 ± 0.01	0.15 ± 0.00	0.15 ± 0.00	21.4
3 (sextet)	0.00	0.03 ± 0.10	336.3 ± 4	0.25 ± 0.01	14.5

The above results show that the co-incorporation of citric acid and glucose affects not only the crystallite size of  $\text{Li}_2\text{FeSiO}_4$  but its crystal structure and microstructure. In fact, the cases that the reflection around  $2\theta = 24.3^\circ$  is either stronger or weaker than that around  $2\theta = 33.1^\circ$  were reported.<sup>9, 43, 44</sup> However, this phenomenon has never been elucidated before, let alone the origin of the change in their relative intensity. Very small crystallites of  $\text{Li}_2\text{FeSiO}_4$  (~20nm) imply that the change is not due to their preferential orientation but structure itself. The change simply in relative intensity is firstly reminiscent of the variations of the intermixing occupancies between Fe and Li. The partial replacement of Fe (Li) by Li (Fe) was also reported as antisite defects in other cathode materials such as  $\text{LiFePO}_4$ , which play a critical role in the electrochemical performance.<sup>45, 46</sup> For  $\text{Li}_2\text{FeSiO}_4$  the effect of the intermixing occupation on its electrochemical performance is not known as yet. Undoubtedly, the correlation between the intermixing occupation and the electrochemical performance should be unveiled. The current study reveals that the quantity of citric acid and glucose influences not only the growth kinetics of  $\text{Li}_2\text{FeSiO}_4$  crystallites but the evolution of the crystalline structure. The larger quantity of citric acid and glucose would form the higher barrier for the diffusion and transport of diversified chemical species in the precursors during the synthesis, and thus causes the shorter range diffusion to limit the species at the nearby crystal sites forming the so called disordered  $\text{Li}_2\text{FeSiO}_4$  due to the intermixing occupation between Fe and Li. The larger amount of citric acid and glucose actually prevents the disordered  $\text{Li}_2\text{FeSiO}_4$  from further ordering by weakening the intermixing. The detailed mechanism behind the formation and growth of  $\text{Li}_2\text{FeSiO}_4$  needs to be further investigated.

### 3.2 Morphological observations

The morphology of all the samples was observed with SEM, which is shown in Figure 1S (supporting information). TEM and HRTEM observations were also carried out on samples C3G8, C6G9 and C6G10, as displayed in Figure 3. SEM images show the large number of agglomerates, and the agglomeration tends to be enhanced as the molar quantity of citric acid and glucose increases. Intriguingly, citric acid has a more crucial role to play in alleviating the agglomeration compared to glucose, which is unambiguously revealed by comparing Figure 1S h, i, j and k, l, m. TEM observations reveal that the agglomerates are composed of nanoscale crystallites in which the size for sample C3G8 is about 30 nm, larger than those for samples C6G9 and C6G10, being consistent with the results from the XRD data in Table 1. HRTEM images suggest good crystallinity of  $\text{Li}_2\text{FeSiO}_4$  nanoparticles, as demonstrated by the clear lattice fringes shown in Figure 3. For sample C3G8 little carbon was found to encapsulate  $\text{Li}_2\text{FeSiO}_4$  nanoparticles. However, for samples C6G9 and C6G10 a uniform layer of carbon films were formed at

the surface. Moreover, some isolated carbon was observed in sample C6G10. This is understandable in terms of the weight percentages of carbon 1.37%, 3.64%, and 4.15% in samples C3G8, C6G9 and C6G10, respectively, which were determined using a carbon and sulfur analyzer.

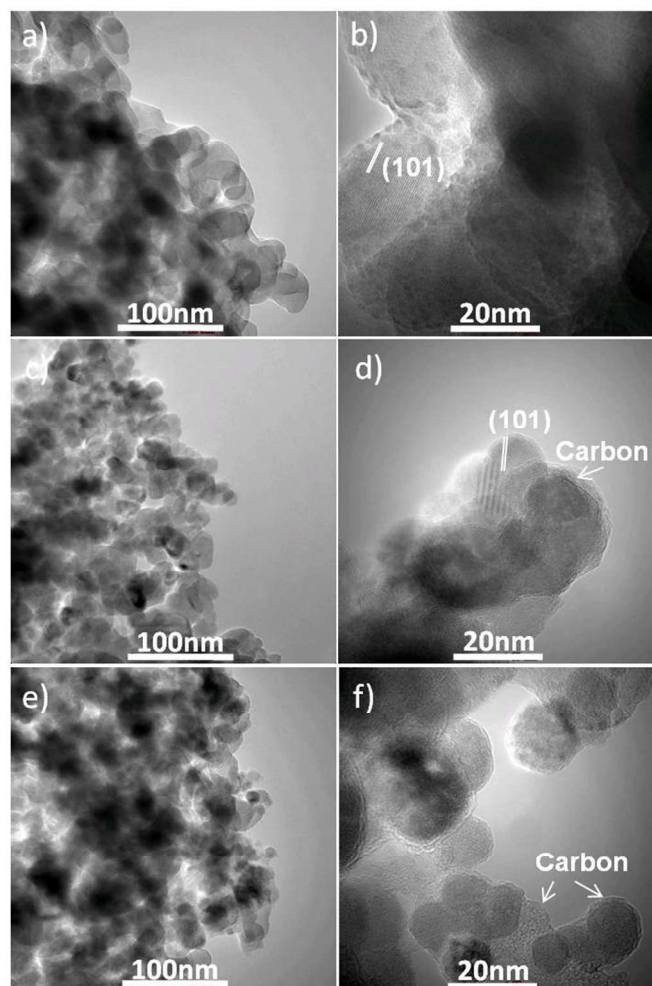


Figure 3. TEM and HRTEM images of samples C3G8 (a), (b), C6G9 (c), (d) and C6G10 (e), (f).

### 3.3 Electrochemical performance

To investigate the influence of citric acid and glucose on the electrochemical performance of  $\text{Li}_2\text{FeSiO}_4/\text{C}$  composites, electrochemical tests were performed. Figure 2S shows the first charge / discharge curves of different  $\text{Li}_2\text{FeSiO}_4/\text{C}$  electrodes at 0.1 C rate over the potential range of 1.5 - 4.8 V. The discharge capacities of samples C3G8, C3G9, C3G10, C3G11, C6G5, C6G6, C6G7, C6G8, C6G9, C6G10, C9G5, C9G6 and C9G7 are 94.9, 102.4, 114.9, 82.8, 57.5, 100.7, 130.3, 135.1, 171.0, 171.0, 152.4, 160.6 and 161.1  $\text{mAhg}^{-1}$ , respectively. The discharge capacity increases firstly with the increased molar quantity of citric acid and glucose, and then decreases. Samples C6G9 and C6G10 exhibit the highest discharge capacities but the former shows smaller polarizations, as indicated by Figure 2S.

Figure 4 shows the charge / discharge curves of sample C6G9 over the different potential ranges, such as 1.5 - 4.8 V, 2.0 - 4.8 V,

# RSC advances

1.5 – 4.5 V, and 2.0 - 4.5 V. The first charge curve over the potential range of 1.5 – 4.8 V displays an apparent voltage plateau followed by an increasing voltage whereas the first discharge curve gives a decreasing voltage. With the increased cycle numbers, the polarization increases significantly with a drop of discharge capacity of about 46 mAhg<sup>-1</sup>, from 171.1 to 125.2 mAhg<sup>-1</sup>, about 27% drop (from the 1<sup>st</sup> to 43<sup>rd</sup> cycle). From 43<sup>rd</sup> to 119<sup>th</sup> cycle, the discharge curve becomes typically capacitor-like, and the capacity decreases by about 40 mAhg<sup>-1</sup>. Another test was taken firstly over the potential range of 2.0 – 4.2 V for two cycles, and then over the range of 2.0 – 4.5 V from the 3<sup>rd</sup> to 43<sup>rd</sup> cycle, and finally over the range of 1.5 – 4.5 V from the 44<sup>th</sup> to 119<sup>th</sup> cycle, as shown in Figure 4 (b). The discharge capacity decreases by about 4 mAhg<sup>-1</sup>, from 125.8 to 122.2 mAhg<sup>-1</sup> after the first 40 cycles, only 3% drop over the range of 2 – 4.5 V. However, from the 44<sup>th</sup> to 119<sup>th</sup> cycle over the range of 1.5 – 4.5 V, the discharge capacity decreases by about 40mAhg<sup>-1</sup>, from 146.4 to 106.6 mAhg<sup>-1</sup>. Therefore, with the discharge cutoff potential of 1.5 V and for the upper cutoff potentials of 4.5 V and 4.8 V, both the discharge capacities decrease by almost the same values (~40 mAhg<sup>-1</sup>) subjected to the same number of cycles. Upon the 119<sup>th</sup> cycle compared to 1.5 – 4.8 V a discharge plateau still remains for 1.5 – 4.5V with a capacity about 30 mAhg<sup>-1</sup> higher. For 1.5 - 4.5 V the charge plateau first levels down and then up again with cycling, and the polarizations are far smaller than those for 1.5 – 4.8 V. This may be closely related to structural changes taking place after the initial charge.<sup>9</sup> Moreover, higher charge cutoff potentials, say 4.8V would not facilitate the electrochemical performance of Li<sub>2</sub>FeSiO<sub>4</sub>, different than refs. 47, 48

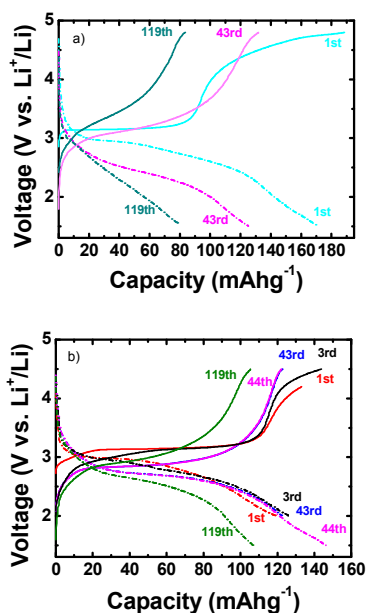
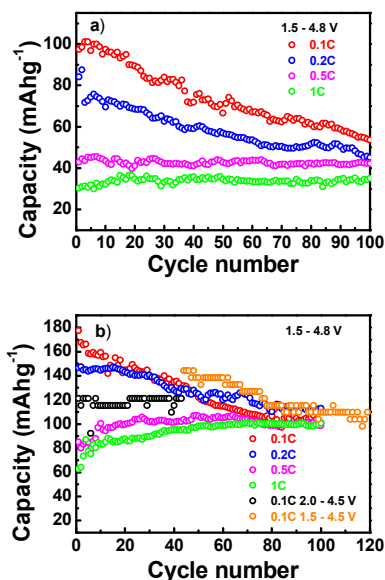


Figure 4. Charge / discharge curves for sample C6G9 at 0.1 C over the potential ranges of 1.5 - 4.8 V (a), 1.5 - 4.5 V, 2.0 - 4.5 V and 2.0 - 4.2 V (b)

The dependence of performance with the cutoff potentials could be rationally explained. The higher charge cutoff potential would force more Li<sup>+</sup> to extract from Li<sub>2</sub>FeSiO<sub>4</sub> which has a higher energy barrier and is an irreversible process. This process probably disrupts partly the structure of Li<sub>2</sub>FeSiO<sub>4</sub> which leads to a severe loss of discharge capacity with the progress of cycling. This is quite true for the severe intermixing occupation of Fe and Li in that Fe at both the

Li and Fe sites would prevent Li<sup>+</sup> from extraction / insertion.<sup>41</sup> The lower charge cutoff potential makes the extraction / insertion of the intrinsic reversible Li<sup>+</sup> easy to be triggered without disrupting the structure. Meanwhile, the intermixing occupation of Fe and Li may create some defects for Li<sup>+</sup> more easily to transport in the structure. After the initial cycles the drop of the charge voltage plateau implies a process of a possible structural rearrangement to a stable structure which is considered to be closely related to the intermixing occupation between Fe and Li.<sup>49</sup> It is worth noting that the Li at both the Li and Fe sites probably contributes to the capacity of Li<sub>2</sub>FeSiO<sub>4</sub>, which needs to be further investigated.

The cycling performance of samples C3G8, C6G9 and C6G10 at various rates over different cutoff potentials is displayed in Figure 5. Sample C6G9 is shown to have the better cycling performance especially at higher rates compared to sample C6G10. The discharge capacity for all the samples tends to decrease both at 0.1 and 0.2 C, and however to increase at 1 C with the increased cycle numbers. This may be related to an improvement of electrical conductivity with further cycling. The discharge capacity of sample C6G9 for a narrower charge and discharge window, say 2.0 – 4.5 V is stable, around 120 mAhg<sup>-1</sup>. However, upon discharging down to 1.5 V, though the capacity increases by about 20 mAhg<sup>-1</sup> firstly it gradually drops back to about 120 mAhg<sup>-1</sup>. Increasing the charge cutoff potential up to 4.8 V would lead to a higher initial discharge capacity over 170 mAhg<sup>-1</sup> followed by a more rapid drop down to about 105 mAhg<sup>-1</sup>. More interestingly, samples C6G9 and C6G10 show lower discharge capacities over the initial cycles at 0.2 C compared to 0.1 C but they were reversed with further cycling. This is not the case for sample C3G8 at all. The discharge capacity at 0.2 C starts to exceed that at 0.1 C at the far earlier cycles for sample C6G10 compared to sample C6G9. This may be a consequence of different kinetics of Li<sup>+</sup> transportation against discharging rates due to their different intermixing occupancies between Fe and Li. For sample C6G10 Li<sup>+</sup> transportation kinetics is more sluggish so that Li<sup>+</sup> cannot rapidly respond to the charging rate even at 0.1 C, especially over the earlier cycles. This is also evidenced by the increasing discharge capacity with increased cycles for sample C6G10, as seen from Figure 5 (c). As far as both the size (smaller) and carbon content (somewhat higher) of Li<sub>2</sub>FeSiO<sub>4</sub>/C particles sample C6G10 is deduced to have a Li<sup>+</sup> transportation kinetics faster than that of sample C6G9. However, this unexpected result could be ascribed to the phase transition via solid solution during charge / discharge, which is influenced more significantly by the higher intermixing occupancies between Fe and Li for sample C6G10.



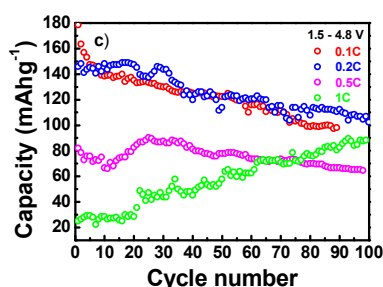


Figure 5. Cycling performance of samples C3G8 (a), C6G9 (b) and C6G10 (c) at different rates and over different charge / discharge cutoff potentials.

Figure 6 gives the cyclic voltammograms of the first three cycles for samples C3G8, C6G9 and C6G10 with a scan range of 1.5 - 4.5 V and a scan rate of 0.5 mV s<sup>-1</sup>. Three samples show basically the very similar profiles with the redox peaks of Fe<sup>2+</sup>/Fe<sup>3+</sup>, as reported<sup>50</sup>. After the first cycle the oxidation peak for three samples obviously shifts to the side of the lower voltage and then tends to move towards the higher voltage again with increased cycles, as revealed by the vertical line segments in Figure 6. The reduction peak for three samples tends to shift to the side of the lower voltage. The obvious drop of the oxidation voltage from the first to second cycle is supposed to be due to a significant structural rearrangement.<sup>50</sup> In addition, the oxidation peak after the first cycle gets narrower whereas the reduction peak becomes a little bit broader with cycles, which is somewhat different from other results.<sup>50, 51</sup> More interestingly, both the oxidation and reduction peaks get broader in the sequence of sample C3G8, C6G9 and C6G10, as shown in Figure 6. The increased breadth of the redox peaks is considered to arise from the increased intermixing occupation between Fe and Li from sample C3G8 to C6G9 to C6G10 derived from the above XRD data. The highest current densities of the redox peaks for sample C6G9 could account for its optimum performance as well.

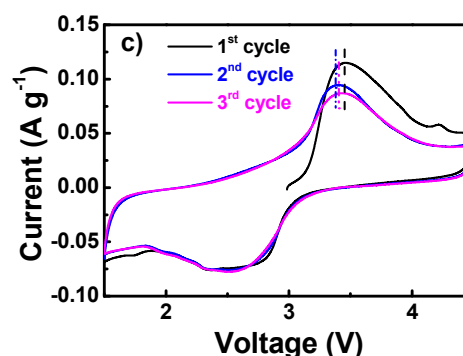
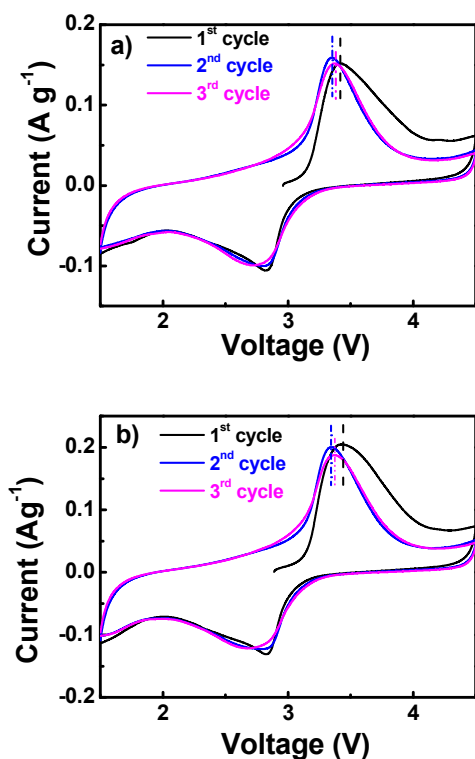


Figure 6. Cyclic voltammograms of the first three cycles for samples C3G8 (a), C6G9 (b) and C6G10 (c), scanning rate: 0.5 mV s<sup>-1</sup>

In order to better understand the improved electrochemical performance of sample C6G9, EIS were recorded for samples C3G8, C6G9 and C6G10, as shown in Figure 7. The impedance spectra exhibit a depressed semicircle in the high-frequency range and a sloping line in the low frequency range. This kind of impedance spectra are typically characterized by the ohmic resistance, charge transfer resistance, and the Warburg behavior.<sup>52</sup> Based on the understanding of the fundamental electrochemical process, an equivalent circuit model is given in the inset of Figure 7. In the model,  $R_s$  is referred to as the resistance of the electrolyte,  $R_1$  and  $CPE_1$  the resistance and capacity of the surface film,  $R_2$  and  $CPE_2$  the charge transfer resistance and capacity, and  $Z_w$  is the Warburg impedance. Some parameters for the model are outlined in Table 4. From Table 4 each kind of resistance or impedance differs for samples C3G8, C6G9 and C6G10. The resistances of the electrolyte are quite small and negligible compared to other resistances. The maximum or total resistance / impedance would determine the electrochemical performance of a sample.<sup>53</sup> Sample C3G8 has the maximum Warburg impedance and charge transfer resistance, also the lowest Li<sup>+</sup> diffusion coefficient, suggesting that its poor electrochemical performance arises from the poor electronic conductivity and poor Li<sup>+</sup> diffusion in the material.<sup>53</sup> The charge transfer resistance decreases from sample C3G8, C6G9 and C6G10, which can be well explained by the change of their carbon contents. Sample C6G9 has the highest Li<sup>+</sup> diffusion coefficient, and exhibits values comparable in charge transfer resistance, surface film resistance and Warburg impedance, and thus shows the optimum electrochemical performance. Sample C3G8 has the lowest Li<sup>+</sup> diffusion coefficient, which may be related to its structure with the least intermixing occupation between Fe and Li, and its largest particle size. An appropriate intermixing occupation between Fe and Li for Li<sub>2</sub>FeSiO<sub>4</sub> could introduce some defects etc. which probably facilitate the diffusion of Li<sup>+</sup> in the lattice, thus increasing the diffusion coefficient of Li<sup>+</sup>. This, along with its lowest carbon content may result in the poorest performance of sample C3G8. Though sample C6G9 has larger particle size (evidenced by both the XRD data and BET data of samples C3G8 (30.28 m<sup>2</sup>g<sup>-1</sup>), C6G9 (51.51 m<sup>2</sup>g<sup>-1</sup>), and C6G10 (51.74 m<sup>2</sup>g<sup>-1</sup>) and lower carbon content compared to sample C6G10 it has better electrochemical performance, particularly rate capability. Its better performance, say, rate capability arises from the highest Li<sup>+</sup> diffusion coefficient, which could be ascribed to an appropriate intermixing between Fe and Li. Obviously, the effect of improvement in electrochemical performance caused by the appropriate intermixing between Fe and Li is dominant over those caused by smaller particle size and higher carbon content. Therefore, an appropriate intermixing occupation

## RSC advances

## ARTICLE

between Fe and Li in  $\text{Li}_2\text{FeSiO}_4$  is found to have no negative influences on its performance, which differs from the traditional viewpoints on other cathodes such as  $\text{LiFePO}_4$ .<sup>54</sup> On the contrary, it increases  $\text{Li}^+$  diffusion coefficient and further improves the electrochemical performance of  $\text{Li}_2\text{FeSiO}_4$ . Furthermore, its effect of improvement in electrochemical performance dominates those caused by somewhat size reduction of particles and a little bit higher carbon content.

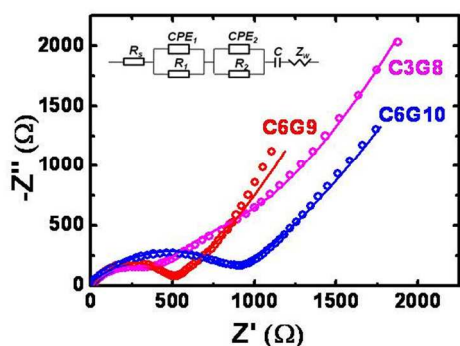


Figure 7. Experimental (dots) and simulated (lines) EIS of samples C3G8, C6G9 and C6G10

Table 4. Impedance parameters and diffusion coefficients obtained from EIS for samples C3G8, C6G9 and C6G10

Samples	$R_s$ ( $\Omega$ )	$R_1$ ( $\Omega$ )	$R_2$ ( $\Omega$ )	$Z_w$ ( $\Omega\text{s}^{-1/2}$ )	$D$ ( $\text{cm}^2\text{s}^{-1}$ )
C3G8	8.3	339.2	248.1	1450.3	$6.983 \times 10^{-17}$
C6G9	6.3	334.6	143.9	244.8	$2.432 \times 10^{-15}$
C6G10	2.0	707.2	107.7	338.2	$1.285 \times 10^{-15}$

#### 4. Conclusions

Nano - sized  $\text{Li}_2\text{FeSiO}_4/\text{C}$  was synthesized using a simple recipe via co - incorporating citric acid and glucose in various molar ratios followed by a two - step annealing. Glucose affects the size of crystallites more effectively and citric acid alleviates their agglomeration. The decreased relative intensity of the reflections around  $2\theta = 24.3^\circ$  and  $33.1^\circ$  with the molar quantity of citric acid and glucose originates from the increased intermixing occupancies between Fe and Li. An appropriate intermixing occupancy would facilitate the performance of  $\text{Li}_2\text{FeSiO}_4$ , which differs from the traditional viewpoints. The underlying mechanism of citric acid and glucose to govern the growth of  $\text{Li}_2\text{FeSiO}_4$  crystallites and the intermixing occupancy between Fe and Li, and their detailed influence on the performance needs to be further investigated. This study proposes a new way to optimize the electrochemical performance of  $\text{Li}_2\text{FeSiO}_4$  by controlling the intermixing occupancies between Fe and Li via the co - incorporation of some organic substances during synthesis.

#### Acknowledgements

Mi, Liu, Tian and Jiang are responsible for the experiments of materials synthesis. Zhang, Gu and Guo contribute to the characterization and analysis of structure. Wang carry out the electrochemical measurements. Sun and Chu complete the

manuscript writing. This work is financially supported by the sub-project ‘‘Exploration of novel cathode materials for lithium ion battery as highly efficient energy storage’’, the project ‘‘Design and Research on the Key Technology of Photovoltaic Demonstration Base’’, and the Knowledge Innovation Program of the Chinese Academy of Sciences, and the Strategic Priority Research Program of the Chinese Academy of Sciences, grant No. XDA09040101.

#### Notes and references

\*corresponding authors: [WGCHU@NANOCTR.CN](mailto:WGCHU@NANOCTR.CN);

[WANGHF@NANOCTR.CN](mailto:WANGHF@NANOCTR.CN); [SLF@NANOCTR.CN](mailto:SLF@NANOCTR.CN)

<sup>a</sup> National Center for Nanoscience and Technology of China, zhongguancun Beiyitiao 11, Beijing 100190, P. R. China.

<sup>b</sup> Department of Physics, Tsinghua University, Beijing 100084, P. R. China

<sup>c</sup> Tsinghua- Foxconn Nanotechnology Research Center, Beijing 100084, P. R. China

Electronic Supplementary Information (ESI) available: See DOI: 10.1039/b000000x/

- J. M. Tarascon and M. Armand, *Nature*, 2001, 414, 359. 2
- J. M. Tarascon, A. S. Gozdz, C. Schmmutz and F. Shokoohi, *Solid State Ionics* 1996, 86, 49.
- A. R. Armstrong and P. G. Bruce, *Nature* 1996, 381, 499.
- N. Yabuuchi, K. Yoshii, S. T. Myung, I. Nakai and S. Komaba, *J. Am. Chem. Soc.* 2011, 133, 4404.
- J. S. Kim, K. S. Kim, W. Cho, W. H. Shin, R. Kanno and J. W. Choi, *Nanolett.* 2012, 12, 6358.
- M. Nishijima, T. Ootani, Y. Kamimura, T. Sueki, S. Esaki, S. Murai, K. Fujita, K. Tanaka, K. Ohira, Y. Koyama and I. Tanaka, *Nat. Comm.* 2014, 5, 4553.
- L. Tao, G. Rouse, J. N. Chotard, L. Dupont, S. Bruyère, D. Hanzel and G. Mali, R. Dominko, S. Levasseur and C. Masquelier, *J. Mater. Chem. A*, 2014, 2, 2060.
- X. L. Jiang, H. Y. Xua, J. Liu, Jian, Yang, H. Z. Mao and Y. T. Qian, *Nano Energy*, 2014, 7, 1.
- A. Nytén, A. Abouimrane and M. L. Armand, *Electrochem. Commun* 2005, 7, 156.
- P. Larsson, R. Ahuja, A. Nytén and J. O. Thomas, *Electrochem. Commun.* 2006, 8, 797.
- F. Zhou, M. Cocossioni, K. Kang and G. Ceder, *Electrochem. Commun.* 2004, 6, 1144.
- M. S. Islam, R. Dominko, C. Masquelier, C. Sirisopanaporn, A. R. Armstrong and P. G. Bruce, *J. Mater. Chem.* 2011, 21, 9811.
- C. Sirisopanaporn, C. Masquelier, P. G. Bruce, A. R. Armstrong and R. J. Dominko, *J. Am. Chem. Soc.* 2011, 133, 1263.
- M. Bini, S. Ferrari, C. Ferrara, M. C. Mozzati, D. Capsoni, A. J. Pell, G. Pintacuda, P. Canton and P. Mustarelli, *Sci. Rep.* 2013, 3, 3452.
- J. Moskon, R. Dominko, R. C. Korosec, M. Gabersek and J. Jamnik, *J. Power Sources* 2007, 174, 683.
- R. Dominko, D. E. Conte, D. Hanzel, M. Gabersek and J. Jamnik, *J. Power Sources* 2008, 178, 842.
- C. Delacourt, P. Poizot, S. Levasseur and C. Masquelier *Electrochem. Solid State Lett.* 2006, 9, A352.
- S. Zhang, C. Deng and S. Y. Yang, *Electrochem. Solid State Lett.* 2009, 12, A136.
- Z. L. Gong, Y. X. Li, G. N. He, J. Li and Y. Yang, *Electrochem. Solid State Lett.* 2008, 11, A60.
- H. J. Guo, K. X. Xiang, X. Cao, X. H. Li, Z. X. Wang and L. M. Li, *Trans. Nonferr. Met. Soc. Chin.* 2009, 19, 166.
- L. M. Li, H. J. Guo, X. H. Li, Z. X. Wang, W. J. Peng, K. X. Xiang and X. Cao, *J. Power Sources* 2009, 189, 45.
- K. C. Kam, T. Gustafsson and J. O. Thomas, *Solid State Ionics* 2011, 192, 356.
- X. Y. Fan, Y. Li, J. J. Wang, L. Gou, P. Zhao, D. L. Li, L. Huang and S. G. Sun, *J. Alloys & Comp.* 2010, 493, 77.

## ARTICLE

- 24 F. Lin, I. M. Markus, D. Nordlund, T. C. Weng, M. D. Asta, H. L. L. Xin and M. M. Doeff, *Nat. Comm.* 2014, **5**, 3529.
- 25 N. Laszczynski, J. Zamory, N. Loeffler, G. B. Cho, G. T. Kim and S. Passerini, *Chem Electro Chem.* 2014, **1**, 1537.
- 26 S. Y. Chung, S. Y. Choi, S. Lee and Y. Ikuhara, *Phys. Rev. Lett.* 2012, **108**, 195501.
- 27 J. L. Yang, X. C. Kang, L. Hu, X. Gong and S. C. Mu, *J. Mater. Chem. A*, 2014, **2**, 6870.
- 28 Z. X. Chen, S. Qiu, Y. L. Cao, J. F. Qian, X. P. Ai, K. Xie, X. B. Hong and H. X. Yang, *J. Mater. Chem. A*, 2013, **1**, 4988.
- 29 Z. Gong and Y. Yang, *Energy Environ. Sci.* 2011, **4**, 3223.
- 30 T. Muraliganth, K. R. Stroukoff and A. Manthiram, *Chem. Mater.* 2010, **22**, 5754.
- 31 D. Jugovi, M. Milovi, V. N. Ivanovski, M. Avdeev, R. Dominko, B. Joki and D. Uskokovi, *J. Power Sources*, 2014, **265**, 75.
- 32 S. Ferrari, D. Capsoni, S. Casino, M. Destro, C. Gerbaldi and M. Bini, *Phys. Chem. Chem. Phys.* 2014, **16**, 10353.
- 33 J. Moskon, R. Dominko, M. Gaberscek and R. C. Korosec, *J. Electrochem. Soc.* 2006, **153**, A1805.
- 34 M. Gaberscek, R. Dominko, M. Bele, M. Remskar and J. Jamnik, *Solid State Ionics* 2006, **177**, 3015.
- 35 R. Dominko, M. Bele, M. Gaberscek, M. Remskar and D. Hanzel, J. M. Goupil, S. Pejovnik and J. Jamnik, *J. Power Sources* 2006, **153**, 274.
- 36 B. Rehani, P. B. Joshi, K. N. Lad, A. Pratap. *Indian J. Pure & Appl. Phys.* 2006, **44**, 157.
- 37 S. Nishimura, S. Hayase, R. Kanno, M. Yashima, N. Nakayama and A. Yamada *J. Am. Chem. Soc.* 2008, **130**, 13212.
- 38 J. Rodriguez-Carvajal, *Fullprof, Program for Rietveld Refinement*, 1997, version 3.7 [J]. LLB JRC
- 39 A. Boulineau, C. Sirisopanaporn, R. Dominko, A. R. Armstrong, P. G. Bruce and C. Masquelier, *Dalton Trans.* 2010, **39**, 6310.
- 40 I. K. Lee, S. J. Kim, T. Kouh and C. S. Kim, *J. Appl. Phys.* 2013, **113**, 17E306.
- 41 G. Krishna, P. Dathar, D. Sheppard, K. J. Stevenson and G. Henkelman, *Chem. Mater.* 2011, **23**, 4032.
- 42 I. S. Lyubutin, P. G. Naumov, B. V. Mill, K. V. Frolov and E. I. Demikhov, *Phys. Rev. B* 2011, **84**, 214425.
- 43 P. Axmann, C. Stinner, M. Wohlfahrt-Mehrens, A. Mauger, F. Gendron and C. M. Julien *Chem. Mater.* 2009, **21**, 1636.
- 44 S. Y. Chung, Y. M. Kim and S. Y. Choi, *Adv. Funct. Mater.* 2010, **20**, 4219.
- 45 P. Axmann, C. Stinner, M. Wohlfahrt-Mehrens, A. Mauger, F. Gendron and C. M. Julien *Chem. Mater.* 2009, **21**, 1636.
- 46 S. Y. Chung, Y. M. Kim and S. Y. Choi, *Adv. Funct. Mater.* 2010, **20**, 4219.
- 47 B. Shao and I. Taniguchi, *J. Power Sources* 2012, **199**, 278.
- 48 D. P. Lv, W. Wen, X. K. Huang, J. Y. Bai, J. X. Mi, S. Q. Wu and Y. Yang, *J. Mater. Chem. A* 2011, **21**, 9506.
- 49 J. Wilcox, S. Patoux and M. Doeff, *J. Electrochem. Soc.* 2009, **156**, A 192.
- 50 A. Nyten S. Kamali, L. Häggström, T. Gustafsson and J. O. Thomas, *J. Mater. Chem.* 2006, **16**, 2266.
- 51 G. Peng, L. L. Zhang, X. L. Yang, S. Duan, G. Liang and Y. H. Huang, *J. Alloy & Comp.* 2013, **570**, 1.
- 52 Z. Yan, S. Cai, X. Zhou, Y. Zhao and L. Miao, *J. Electrochem. Soc.* 2012, **159**, A894.
- 53 P. Ghosh, S. Mahanty and R. N. Basu, *J. Electrochem. Soc.* 2009, **156**, A677.
- 54 L. Wang, X. M. He, W. T. Sun, J. L. Wang, Y. D. Li and S. S. Fan, *Nano letters* 2012, **12**, 5632.